Fortgeschrittenenpraktikum K2: Spectroscopy of 2D semiconductors

1 Basics

This chapter gives is a summary of the pyhsical basics underlying the experiment of this practical course. First we introduce the fundamental properties of semiconductors and their optical properties. The second section introduces the group of transition metal dichalcogenides (TMDs). These two dimensional semiconductor layers have been under intense investigation in recent years because of their unique properties making them a promising candidate for future opto-electronic applications.

1.1 Optical properties of semiconductors

The following figure 1.1 shows the characteristic band structure of metals, semiconductors and insulators at a temperature of T = 0K.
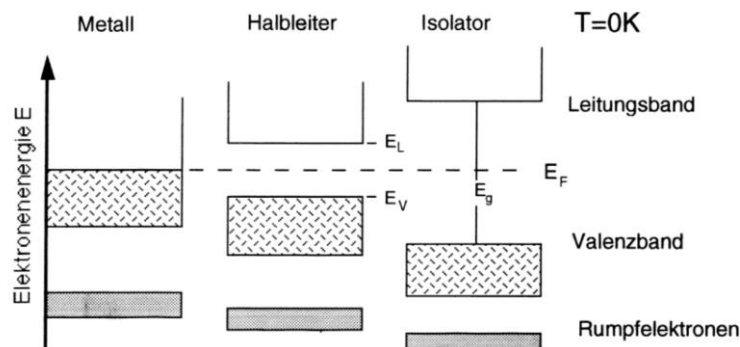

Abbildung 1.1

The Fermi energy EF is the energy up to which the allowed electron states are occupied at T = 0K. The energetically highest band which is completely filled by electrons is called valence band, the lowest not entirely filled band is the conduction band. A fully filled band as well as an empty band does not contribute to electric conductivity. Such a material is called insulator. The energy difference between the upper edge of the valence band (called valence band edge EV) and the lower edge of the conduction band (called conduction band edge EC) is termed band gap Eg . In case of Eg < 5eV finite temperatures cause a thermal broadening which is determined by the Fermi-Dirac distribution f(E,T)

$$f(E,T) = \frac{1}{exp\left(\dfrac{E-\mu}{kT}\right) + 1} \tag{1.1}$$

where k is the Bolzmann constant and T is the absolute temperatur Fig. 1.2 µ is the chemical potential that is defined as the energy where f(E,T) = 0.5 (with µ(T=0) = EF).
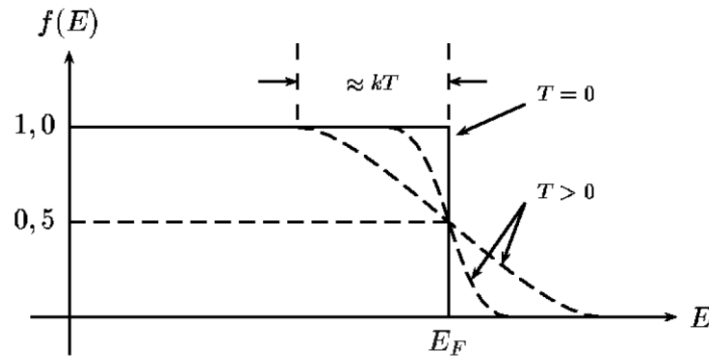

Abbildung 1.2

Therefore statistically there is always a finite fraction of valence band electrons located in the conduction band at finite temperatures. In other words at finite temperatures there are thermally occupied states in the conduction band. This activated electrons as well as the correspondingly created holes in the valence band contribute to electric current. Such a material is called semiconductor. Its electric resistance decreases with increasing temperatures (in contrast to metals).

Optical transitions are normally either interband transitions, between different energy bands, or intraband transitions, within one band. They are caracterized by a particle moving from an occupied to an empty state. Optical absorption is commonly refered to as interband transitions from the valence to the conduction band. Photon emission is mostly caused by transitions from the conduction to the valence band (recombination). This emission is also called photoluminescence (PL). In semiconductors or insulators photoemission is possible only above a certain energy corresponding to the band gap energy Eg . Below this energy the bulk material is optically transparent (referred to as absorption edge). Intraband transitions often involve phonon interactions (a phonon is the quasi-particle of crystal lattice oscillations) and thus occur without photon emission. Hence intraband transitions are commonly not observable in photoluminescence spectroscopy.

In a typical PL spectroscopy experiment the semiconductor is illuminated by monochromatic light with a photon energy above the bandgap ($\hbar\omega > E_g$) . Absorption within the material creates hot electrons and holes which quickly relax to the lowest energy states within the bands by phonon-phonon or electron-electron interaction (electrons relax to

the lowest conduction band states, holes to the highest valence band states). The attrac-
ting electrostatic force can now lead to a bound state between an electron and a hole.
This electron-hole pair is called exciton. The exciton lifetime of typically about 1ns by
far exceeds the characteristic relaxation times (of the order of ps). Semiconductors show
a direct bandgap if the bandgap energy is determined by conduction band and valence
band states having the same k-vector and therefore being located at the same place of
the Brilloin zone - see Fig. 1.3. In direct bandgap semiconductors exciton recombination
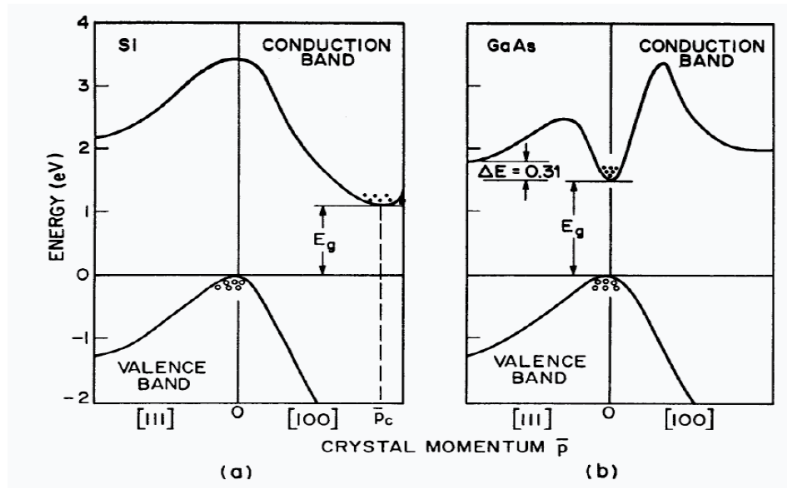is accompanied by strong luminescence.

Abbildung 1.3

The energy of a radiated photon is exactly the difference between the band gap and the
exciton binding energy. The electron-hole binding within the exciton is similar to that of
the electron and proton of the hydrogen atom. Merely the screening of the electron-hole
interaction caused by the surrounding crystal lattice with dielectric constant ϵ has to be
taken into account as well as the deviating particle masses within the crystal. Latter is
accomplished by replacing the mass m by an effective mass m* containing all the correc-
tions imposed on the motion of electron and hole inside the semiconductor. Including this
adjustments the calculations are identical to that of free particles. Hence for an infinitely
large crystal in 3 dimensions the binding energy of the exciton ground state (n = 1) is
given by:

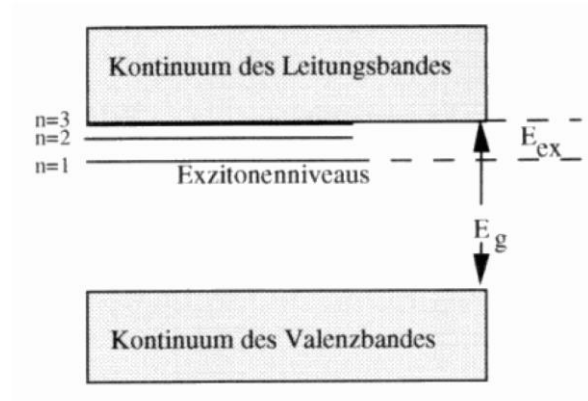$$E_B = \frac{m^* e^4}{8\epsilon^2 \epsilon_0^2 h^2} \qquad (1.2)$$

Abbildung 1.4

1.2 Transition Metal Dichalcogendides

Transition metal dichalcogenides (TMDs) are a group of semiconducting materials of the form MX_2, where M is a transition metal of group VI such as Molybdenum (Mo) or Tungsten (W), and X denotes a chalcogen atom such as sulfur (S), selenium (Se) or tellurium (Te). This chapter gives a short introdction to this group of materials.

1.2.1 Crystal and Band Structure

The crystal structure of TMDs exhibits a stacking of layers weakly coupled to each other by van der Waals forces, which makes it feasible to separate single layers from the bulk crystal by mechanical exfoliation and create heterostructures from these layers, as shown in Fig. 1.5.

TMDs feature a transition from an indirect semiconductor in bulk material to a direct semiconductor in the limit of a single layer [2]. This results in a much stronger photoluminescence signal for TMD monolayers as explained in the previous section. Due to the electron–hole pairs created by optical excitation are confined in two dimensions, and there are no neighboring atoms in vertical direction, the dielectric screening is strongly reduced. For this reason excitons in TMD monolayers have large binding energies of up to several hundred meV, which makes them observable even at room temperature, which we aim in this practical course.

Like in graphene, atoms in TMD monolayers are arranged in a hexagonal lattice (the right panel in Fig. 1.6). The Brillouin zone of monolayers MX_2 is hexagon, and, as in graphene, the most interesting optical and transport effects correspond to particles with momentum at $K^{\pm}$ points of the Brillouin zone shown in the left panel of Fig. 1.6.

In contrast to graphene, where the valence band and conduction band overlap at these points, a gap opens at the K points in the TMD and a direct band gap is formed. Another important difference from graphene is the exceptional strength spin–orbit interaction in
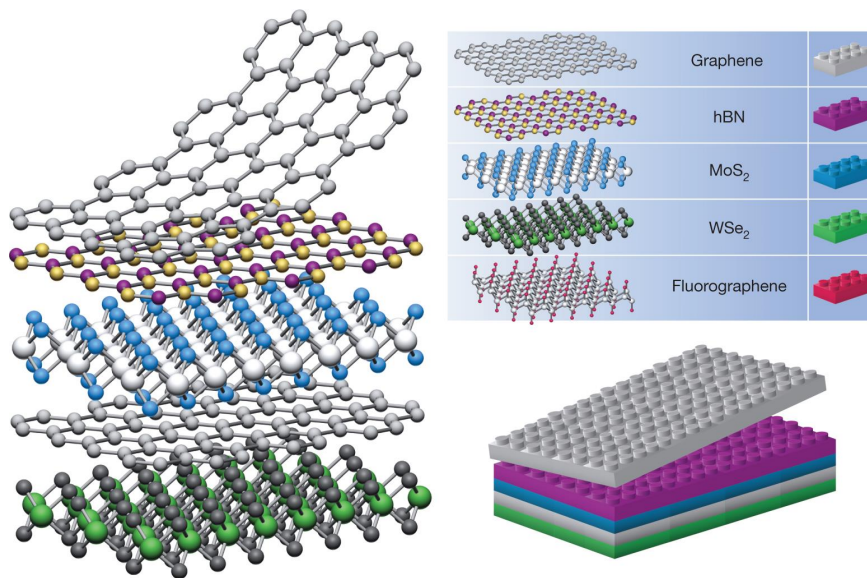
Abbildung 1.5: 2D crystals can be stacked as Lego blocks, resulting in variety of layered heterostructures. Adapted from Ref. [1]
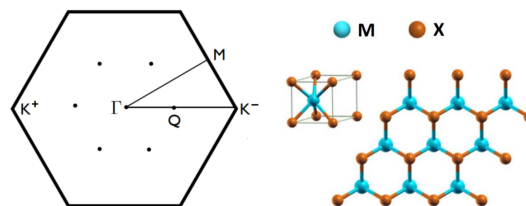

Abbildung 1.6: Brillouin zone with the designation of high-symmetry points and the schematic representation of the crystal structure of an MX_2 monolayer.

MX_2, due to the significant atomic weight of transition metals. This circumstance leads to the removal of the spin degeneracy of the states of the valence band and the conduction band in the monolayers at K points the Brillouin zone, and the spin–orbit splitting of the valence band is hundreds of meV, and the conduction bands are from units to tens of meV [3]. The signs of spin–orbit splittings in the K^+ and K^- valleys are opposite, so the ground state of the electron and the hole in each valley has a certain spin.

For most of TMD bilayers the exciton ground state is momentum-indirect, because usually the conduction band minimum shifts in direction $K \to Q$, whereas the valence band maximum appears at Γ point [4]. For example, the monolayer $MoSe_2$ from *ab initio* calculations is the direct semiconductor with the lowest-energy exciton at 1.8 eV (see Fig.1.7 left panel), whereas for the bilayer $MoSe_2$ the direct exciton at K-point is red-shifted, due to the bandgap renormalization, and has energy of 1.76 eV, but the lowest-energy excitons are momentum-indirect and corresponded to $K \to Q$ and $\Gamma \to Q$ transitions

(see Fig.1.7 right panel). The optical transitions involving excitons direct in momentum space with carriers from the K points can be broadened compared to the monolayer case due to relaxation towards the lower-lying indirect bandgap.
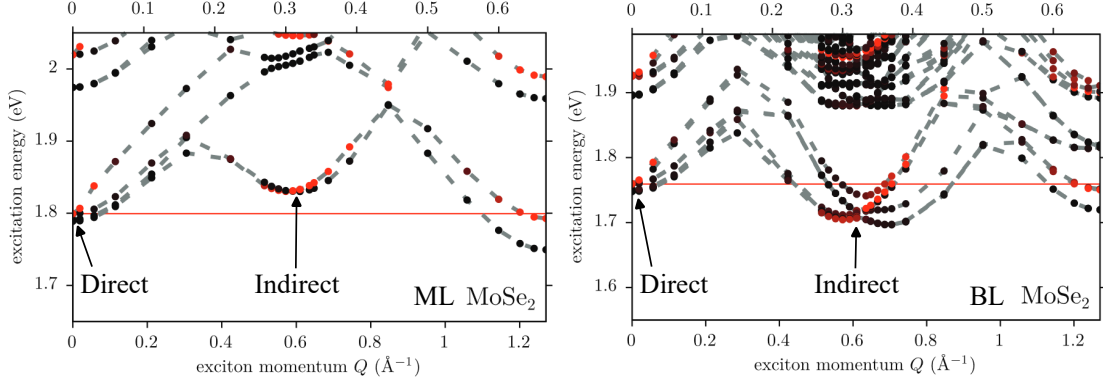

Abbildung 1.7: Exciton band structure of $MoSe_2$ monolayer and bilayer. The grey dashed lines are a guide to the eye for the dots which denote the calculated peaks. The color corresponds to the expectation value of the dipole operator ranging from red (high amplitude) to black (zero amplitude). The horizontal red line shows the energy of the lowest direct-momentum exciton. For the ML the direct-momentum transition is energetically lower than the momentum-indirect transition, the BL shows reversed behaviour. Adapted from Ref. [4]

1.2.2 Coulomb Interaction in thin Films

In contrast to quantum wells made of III-V and II-VI semiconductors, structures based on TMD monolayers are characterized by a significant contrast of dielectric properties. This can be most pronounced for suspended monolayers surrounded by air or vacuum, since the dielectric permittivity of bulk crystals MX_2 is about 10 and in this case significantly exceeds the dielectric permittivity of the environment 1. The potential of the electrostatic field created by the point charge in a thin film placed between two bulk dielectrics was calculated in Refs. [5, 6]. This potential differs from standard Coulumb form

$$V(\rho) = -\frac{\pi e^2}{2\varepsilon \rho_0} \left[H_0 \left(\frac{\rho}{\rho_0} \right) - Y_0 \left(\frac{\rho}{\rho_0} \right) \right], \tag{1.3}$$

where e is the electron charge, ρ_0 is the screening length, ε is the effective dielectric constant, and $H_0(x)$ and $Y_0(x)$ are Struve and Neumann functions.

The binding energy of an exciton in standart bulk semiconductors is in the order of 1 to 10 meV. In low-dimensional structures, the binding energy increases owing to the localization of an electron and hole in one or several spatial directions and, correspondingly, to an increase in the Coulomb attraction of charge carriers (see Fig. 1.8). Thus, the binding energy of excitons in two-dimensional semiconductors can reach already hundreds of meV, which is sufficient for investigating exciton effects at room temperature.
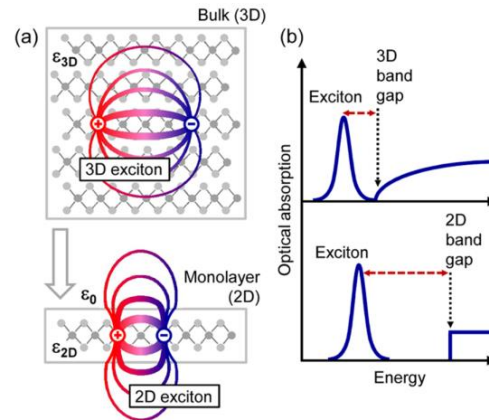
Abbildung 1.8: Schematic illustration of the exciton dielectric screening (a) and the exciton binding energy in bulk and monolayer TMD crystals. Adapted from Ref. [7]

1.2.3 Spectral Lineshape of an Exciton Transition

The optical response of an exciton which is resonantly excited by in-plane polarized light in a two dimensional semiconductor is nothing else than an oscillating dipole and can be therefore discussed by the harmonic oscillator model. Hence, a momentum and spin-direct optical transition manifests as a lorentzian peak in the reflection spectrum with resonance energy E_0 corresponding to the excitonic band gap of the transition. the reflection coefficient r is given by

$$r = \frac{i\gamma_r/2}{E_0 - E - i\gamma_h} \tag{1.4}$$

and the absorption around the resonance is calculated as $A = 1-|r|^2-|t|^2$. The intensity of the peak is a measure for the oscillator strength of the transition, which is a function of its radiative decay rate γ_r. The homogenious linewidth of the resonance corresponds to the total decay rate γ_h of the optical excitation and is a composition of γ_r, the non-radiative decay rate γ_{nr} and the pure dephasing rate γ_d of the transition:

$$\gamma_h = \frac{\gamma_r + \gamma_{nr}}{2} + \gamma_d \tag{1.5}$$

The first two components, γ_r and γ_{nr}, define the decay of population from the excited exciton state to the ground state respectively via radiative recombination and non-radiative recombination corresponding to trapping by defects, relaxation to other exciton states through e.g. electron-phonon sacttering or non-radiative Auger recombination. The pure dephasing rate γ_d corresponds to any mechanism that breaks the coherence between the exciton state and the ground state [8].

Strain effects and local changes in the dielectric environment can lead to variations of the exciton resonance energy, which gives an inhomogenious contribution γ_{inh} to the linewidth

of the resonance. Considering this effect of inhomgenious broadening the absorption peak is not of pure lorentzian lineshape but can be fitted by a convolution of a lorentzian function with linewidth γ_h and a gaussian function with linewidth γ_{inh}. The samples treated here are encapsulated by atomically flat hexagonal boron nitride (hBN) which strongly reduces the inhomgenious broadening within the optical spotsize compared to the thermally broadened homogenious resonance at room temperature. For this reason we neglect the effect of inhomgenious broadening in the scope of this course.

1.2.4 Charged Excitons (Trions)

In the presence of free charge carriers, an electron-hole pair can contact a resident electron or hole and form a three-particle complex — trion, or a charged exciton (see Fig. 1.9). X^+ and X^- are trions formed from two holes and one electron and one hole and two electrons, respectively. These complexes are analogous to hydrogen-like ions H^+ and H^-. In bulk semiconductors, the binding energy of trions is very small, about 1/10 of the exciton binding energy, i.e., units of meV. With a decrease in the dimension of the system and the transition from bulk material to two-dimensional systems the role of the Coulomb interaction is increasing.
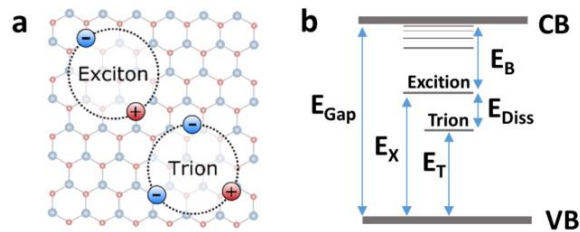

Abbildung 1.9: (a) Exciton and trion formed from one hole and two electrons electrons. (b) Energy order of quasipartices, exciton, and trion.

The increase of the role of Coulomb attraction in monolayers of transition metal dichalcogenides leads to a significant increase in the binding energy of trions. Positively and negatively charged excitons with binding energies of the order of $E_{\text{Diss}} = 30$ meV were found in the TMD monolayers [9]. The typical energy order of electron–hole quasiparticels, exciton, and trion is depicted in Fig. 1.9. Hence, in the presence of free electrons in the system, the new excitonic ground state is a trion state with binding energy increased by E_{Diss}.

2 Experimental Setup and Measurement Techniques

This chapter gives an overview of the experimental platform of this practical course, its functionality and the relevant experimental techniques.
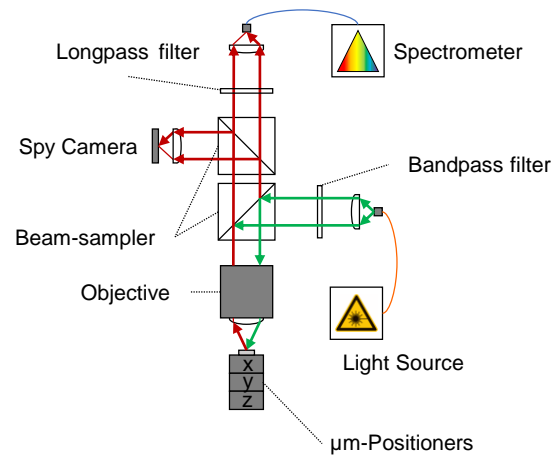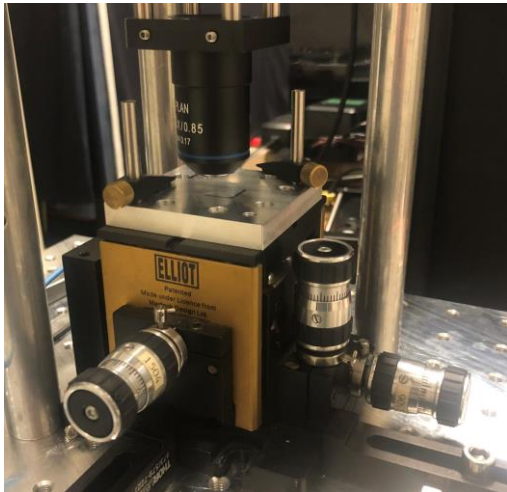
2.1 Confocal microscope

Abbildung 2.1: **left** Image of the micrometer translation stage for sample (x/y) and focal (z) positioning. **right** schematics of the confocal microscope arrangement. The path of the excitation beam coming from a multimode fiber is indicated by green colored arrows while red arrows show the path of the detection beam ending up in a single mode fiber, which guides the light to spectrograph.

The schematics on the right side of fig.2.1 shows the composition and working principle of the confocal microscope which represents the working platform of this practical course. A collimator lens collects light from a point-like source (fiber core of the excitation fiber) and guides the beam to a beam-sampler (90 % Transmission and 10 % Reflection) refelcting a fraction of it into a objective. The latter focuses the light onto the sample substrate leading to an reduced image of the illuminated core of the excitation fiber on the surface of the substrate. The spot size of the image can be estimated from the magnification in a

2-lens system:

$$\frac{d_o}{d_i} = \frac{f_i}{f_o} \tag{2.1}$$

with the size of an object d_o and its image d_i and the focal length f_o and f_i of the respective imaging lens. We use a multimode optical fiber with a core diameter of 50 μm for excitation. Light reflected or emitted from the sample is collected by the objective, mostly transmitted through the beamsampler and focused onto the fiber-core of the detection fiber, which guides the light to a spectrograph for spectral analysis. For detection we use a single-mode optical fiber with a fiber core of a few micrometer. Both collimaters in the detection as well as the excitation arm of the setup are achromatic lens systems with entrance aperture $D = 4.7$ mm and numerical aperture $NA = 0.13$, the objective is a 60x (M) infinity-corrected achromatic microscope objective with $NA = 0.85$ and reference focal length/lens tube length $L = 180$ mm. The effective focal length (f) of an objective relates to the above given parameters in the following ways:

$$NA = \frac{D}{2f} \tag{2.2}$$

$$f = \frac{L}{M} \tag{2.3}$$

Light from the excitation fiber and reflected from the sample surface can only be coupled efficiently into the single mode detection fiber if the image of the detection fiber core lies within the region illuminated by the image of the excitation fiber core on the sample surface as can be seen in Fig. 2.2.

To look at different positions on a sample of interest with a confocal microscope it is placed on a xyz-translation stage as shown on the image on the left side of fig. 2.1. The stage allows for translating the focus of the beam across the sample with submicrometer precision over a range of several millimeter.
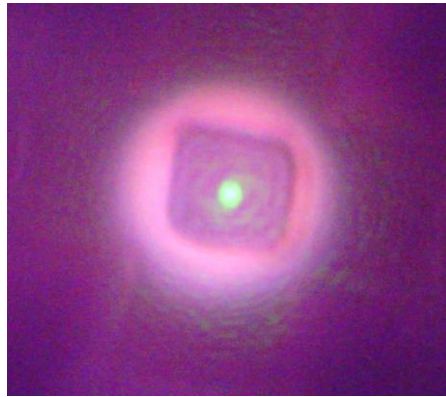
Abbildung 2.2: Image detected by the spy camera showing two spots on the sample surface in the focal plane of the setup. The large one is the image of the core corresponding to the multimode excitation fiber, the small one is the image of the detection single mode fiber core, which is not coupled to the spectrometer in this case but to a green laser. The dark rectangle illuminated by the excitation spot corresponds to a gold chessboard pattern on the SiO_2 surface.

2.2 Sample

In this course, a monolayer and a bilayer $MoSe_2$ are to be investigated by means of optical spectroscopy. Fig. 3.1a shows an optical image of the sample. The different regions of interest are framed by gold markers for better orientation. Fig.3.1b shows microscope images with 50x magnification of the monolayer and the bilayer region, respectively. Both TMD layers are encapsulated with hexagonal boron nitride (hBN) from the top side which protects the TMD layers against degradation at ambient air and prvoides an atomical flat and homogenious dielectric environment. The stacks are placed on a Si/SiO_2 wafer as illustrated in Fig. 3.1c. In addition to the TMD heterostacks the sample features a region (III) with a gold chessboard pattern, which will be used to estimate the scale of the sample expansion. All the gold structures are fabricated by standard photolithography.

2.3 Resolution

In order to attribute certain spectral features to a position on the sample it is important to know the spatial resolution of the detection spot in the focal plane. Figure 2.3 explains the experimental procedure to determine the focal spotsize. Scanning the focal spot across a sample with an atomically sharp edge between two areas of different reflectivity and monitoring the reflected light yields an intensity profile as shown in the upper panel on the right side of Fig. 2.3. The change of Intensity at the edge calculated as the derivative

of the intensity profile is a measure for the resolution of the optical spotsize provided that the expansion of the edge is much smaller than the optical spotsize. The resolution is quantified by extracting the full-width at half-maximum (FWHM) of a gaussian fit to the derivative of the intensity trace.
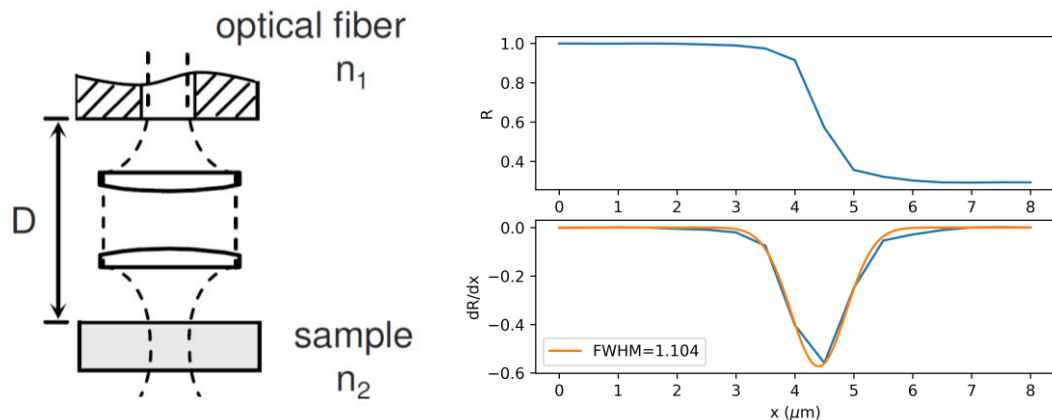

Abbildung 2.3: **left** Schematic of optical imaging of the fiber core of the detection/excitation fiber onto the sample surface. **right** Example for determining the optical resolution. Upper panel: Normalized reflection of the excitation laser from the sample as a function of the x-translation at an atomically sharp edge of a hBN flake. Lower panel: derivative of the normalized reflection trace (blue) and the corresponding fit with Gaussian function (orange). The resolution corresponds to the averaged full-width at half-maximum FWHM $= 1.1 \ \mu$m

2.4 Spectrometer

Figure 2.4 shows a schematic view of a typical spectrometer. The light source which is investigated by the spectrometer (in this case end of the detection fiber) is focused by a lens on the entrance slit of the spectrometer. The width of the slit opening is adjustable with the aid of a micrometer screw (10μm/Skt). The slit is located right at the focal length of the spherical mirror S1 that collimates the incoming light and directs it to the diffracting grid. The focal length of each spherical mirror is 320 mm. The employed grid has a lattice constant of 1200 lines per mm, a reciprocal linear dispersion of 1.9 nm/mm and can be used in the wavelength range of 500 - 1100 nm. The transmission of the spectrometer is 50%. The incident light is diffracted as shown in Fig.2.5.

This yields the situation depicted in Fig. 2.6.

In case of incident polychromatic light the actual lattice position determines the wavelength range which is deflected to the spherical mirror S2. The detector is located right at the focal length of S2. Normally the lattice is placed so that the diffraction of the first order
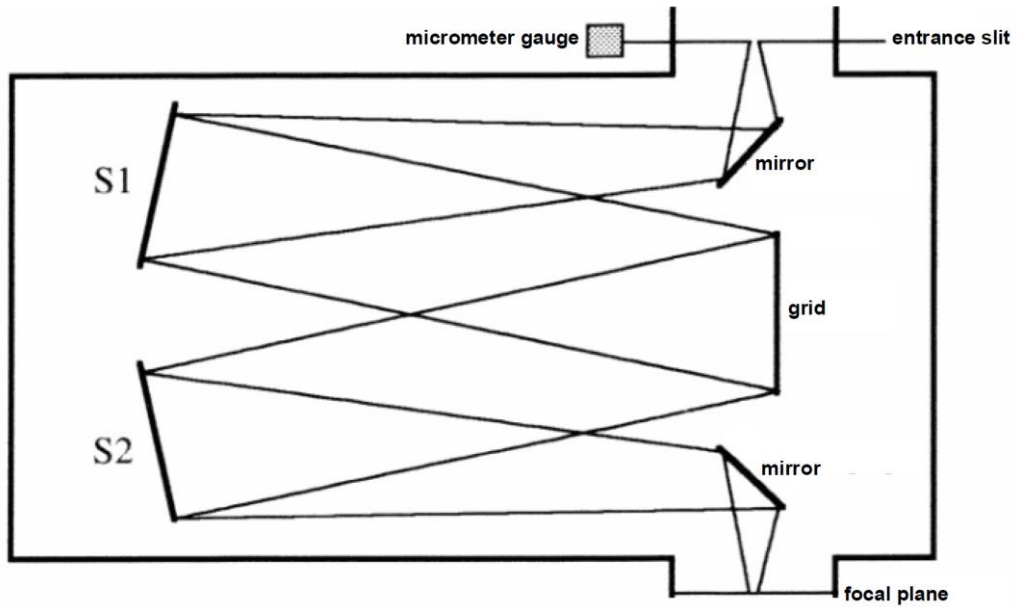
Abbildung 2.4: Optical beam path of a spectrometer

(m=1) is guided onto the detector. The higher order diffractions usually carry strongly decreased light intensity compared to the first order and consequently are virtually not useful experimentally. The lattice position can be adjusted by a screw by hand to tune the wavelength wavelegnth focus onto the center of the detection device.

Abbildung 2.5: Spectrometer grid deflection

Abbildung 2.6: Spectrometer grid deflection orders

2.5 CCD detector

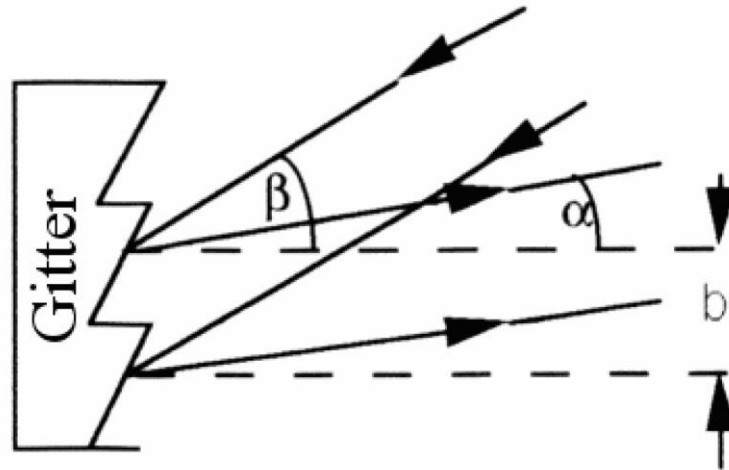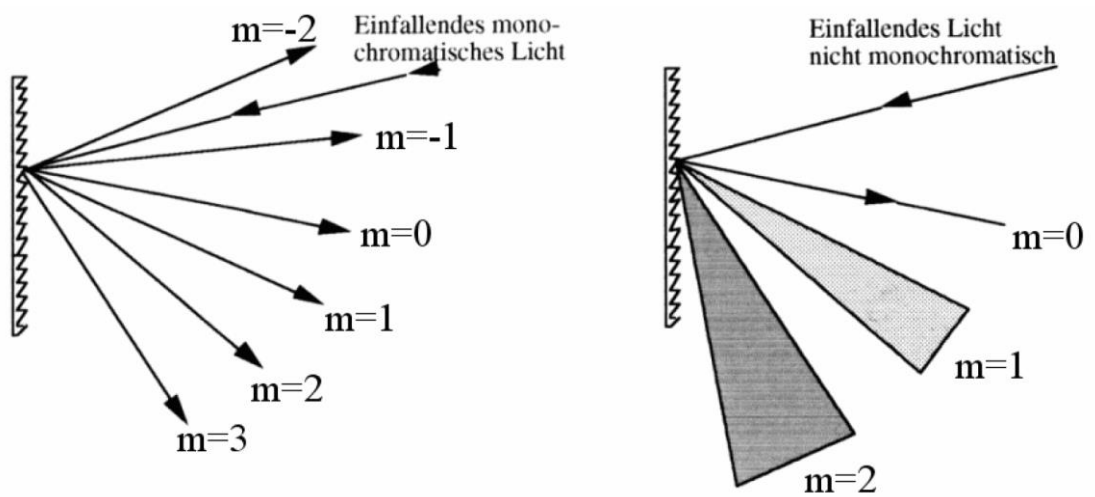Charge Coupled Devices (CCDs) are detectors made from semiconducting n-p-doped silicon layers to which a grid of micro electrodes is attached (Fig. **??**). A proper voltage applied to a micro electrode yields a quantum well potential structure below the electrode. Electrons generated by the photoelectric effect can be captured there. The read-out process involves a clocked change of the local potentials which can shift traped charges in between adjacent potential wells. At the edge of the CCD detector the charge of each row is read out separately, electronically amplified and digitized by an A/D converter.
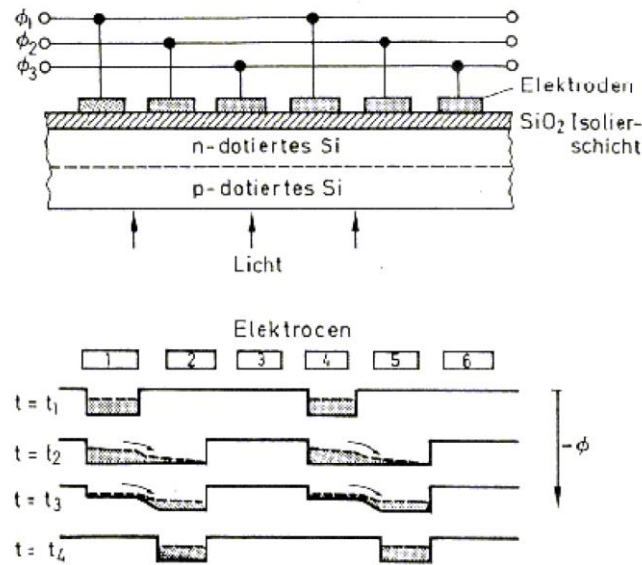

Abbildung 2.7: Schematic of the working principle of a CCD detector.

The main advantage of a CCD compared to a photo multiplier is the possibility of multiplexing. Every pixel of the CCD chip detects simultaneously without reducing spectral resolution or intensity as the entrance slit is imaged onto the detector. Typical widths of the slit window are in the range of 10-20 μm which is about the size of each CCD pixel. In case of using a photo multiplier it would be necessary to adjust the width of the beam exit aperture to the same size too in order to avoid decline of spectral resolution. And on the other hand operating with a CCD device gains intensity since it features an increased quantum efficiency. Nowadays photomultiplier are predominantly used if high temporal resolution is required which a CCD cannot deliver without additional technical aid due to the quite time-consuming read-out process in the order of milliseconds.

The following obstacles have to be taken into account using a CCD detector device:

- All charge-controlled detectors must be cooled in order to minimize thermal noise. Typical target temperatures for spectroscopy applications are in the range of 140 - 200 K. If it would be cooled down further the relative sensitivity would drop as well which would only allow to detect sources of higher luminosity (e.g usage in cameras).

- Additionally to thermal noise the signal is affected by noise emerging from the read-out process of the amplifier. However there has been achieved significant progress eliminating this noise contribution so that it is negligible nowadays.

- The doping of the detector cannot be flawless in either case. Thus a CCD chip can always contain defective pixels which lead to signal loss even if the read-out process would have an efficiency of 100%. Even whole pixel lines can be defective. Those pixels are damaged permanently.

- Images aquired with long integration times can particularly be distorted by so-called spikes which result from strong local electric charge accumulation within CCD pixels. The cause can be natural radioactivity in particular glasses used for the devices or cosmic radiation originating from collisions of high-energy particles from space with molecules of the earth's upper atmosphere („cosmics"). Spike events may be compensated by redundant data accumulation.

The cooled CCD camera which is attached to the spectrometer has a resolution of 1024 x 256 pixels. The edge length of each pixel square is 26 μm yielding a total photo-sensitive area of 26,6 x 6,6 mm^2. In order to measure one (1d) spectrum each final pixel information can stem from all 256 vertically stacked pixels of the chip (called 'binning' of the chip) which enhances the signal-to-noise ratio. For instance in case of purely white noise it would be increased by a factor of sqrt(256) = 16 as the mean signal increases by a factor of 256 in contrast to a fluctuation amplitude gain of 16. The possible maximum number of electrons storable in one potential well till leakage to adjacent wells occurs is crucial for the dynamic range of a camera. In case of horizontal read out the capacity of the read-out register is essential which typically is 105 electrons. A high-efficiency CCD as used in this practical course costs about 30.000 €! The CCD chip is located in the focal image plane of the spectrometer whereby a minimal line width of around 3 pixels is attained. At 800 nm the total wavelength range of a single spectrum is hence 50 nm. The chip is thermoelectrically cooled down to -70°C via the Peltier effect to reduce the contribution of thermal noise. The total camera noise N consists of three parts and can be written as

$$N^2 = N_R^2 + N_D^2 + N_S^2 \tag{2.4}$$

N_R is the read-out noise emerging while reading out and amplifying the charge signal of each camera pixel. For the used camera here it is at maximum 10 counts per read out for the entire device. N_D is the noise level by the dark current that occurs as even without incident photons charges can be accumulated in each pixel. Finally N_S is the noise of the measured signal itself (Photons obey Poisson statistics). The dark current decreases exponentially with decreasing temperature. At -70°C it is less than 1 electron per second. The camera has a quantum efficiency of about 0.9 for the incident wavelength range of 600nm to 900nm.

The read-out electronic circuit acquires every single spectrum (intensity versus pixel number) from the CCD chip one by one. Intrinsically no information regarding the actual wavelength is delivered. This must be executed afterwards using the so-called mid pixel number which refers to the particular pixel (line) of the CCD chip where the wavelength which was set at the sprectrometer is incident.

2.6 Types of Optical Measurements

In the framework of this course we use two different optical measurement techniques to probe the excitonic transitions of the TMD sample - reflection of a broadband white light

source and photoluminescence measurement after excitation with a narrow band laser. The light reflected/emitted from the sample is collected and guided to an optical spectrometer, where it is dispersed and recorded by a CCD (Charge Coupled Device) detector for spectral analysis.

2.6.1 Photoluminescence

Illuminating the sample with light of energies larger than the band gap of the semiconductor material creates free electrons in the conduction band leaving holes in the valence band. Electrons and holes can lose energy by phonon interactions and relax to the lowest possible energy states where they can form a bound state of electron(s) and hole(s) called exciton. After a mean lifetime τ the exciton's electron can recombine with its hole radiatively. The corresponding decay rate is defined as $\gamma=\hbar/\tau$. The energy of the emitted photoluminescence light is equal to the difference of the energies of the consisting charged particles minus their exciton binding energy.

2.6.2 Resonant Reflection Spectroscopy

The absorption behaviour of a semiconductor material can be investigated via reflection measurements under resonant excitation. For this type of measurement we use a halogen lamp, which is characterized by a broad band and smooth intensity profile in a wavelength range between 400nm and 2000nm covering the relevant ground state excitations of the TMD monolayer. To extract the absorption spectrum of the sample, we calculate the differential reflection (DR) between a reflection spectrum R_0 measured at a reference position next to the monolayer sample and a reflection spectrum R on the sample and normalize by the reference signal:

$$DR = \frac{R - R_0}{R_0} \qquad (2.5)$$

To extract important parameters such as the oscillator strength and decay rates of the resonance we need to trace back the shape of the DR spectrum to a lorentzian lineshape, which is expected for a two level exciton system as introduced in the previous chapter. This can be done by directly fitting the observed DR spectrum with a lorentzian function. However, the peaks found in differential reflection will not necessarily show a perfect lorentzian profile, but exhibit asymetric lineshapes and even negative amplitude. This asymetry at the resonance results from interference of photons reflected at the TMD monolayer and the surfaces of the adjacent dielectric layers of the hBN flakes and the SiO$_2$ substrate.

The following paragraph will give a short introduction for motivated readers how to extract the lorentzian parameters from an asymetric differential refelction spectrum. We will provide a python script in the supplementary to try out the procedure on the experimentally observed data. The absorption as a function of frequency of an isolated TMD monolayer is directly related to the imaginary part of the *susceptibility* of the material

$$\chi(\omega) = \chi'(\omega) + i\chi''(\omega) \qquad (2.6)$$

The DR spectrum is not the absorption $\text{Im}[\chi(\omega)]$ but rather $\text{Im}[\psi(\omega)]=\text{Im}[\exp(i\alpha(\omega))\chi(\omega)]$. Interference of reflections at different surface of the sample lead to a phase shift $\alpha(\omega)$. We

assume α to be not dependent on the wavelength, in first order, for simplicity. So we have

$$\psi(\omega) = \psi'(\omega) + i\psi''(\omega) = \psi'(\omega) + iDR(\omega) \tag{2.7}$$

and

$$Im[\chi(\omega)] = Im[exp(-i\alpha(\omega))\psi(\omega)] = cos(\alpha)\psi''(\omega) + sin(\alpha)\psi'(\omega). \tag{2.8}$$

The dispersion and absorption of the susceptibility are connected via *Kramers-Kronig relations*:

$$\psi'(\omega) = \frac{2}{\pi}CH \int_0^\infty \frac{\tilde{\omega}\psi''(\tilde{\omega})}{\tilde{\omega}^2 - \omega^2}d\tilde{\omega} \tag{2.9}$$

$$\psi''(\omega) = -\frac{2}{\pi}CH \int_0^\infty \frac{\omega\psi'(\tilde{\omega})}{\tilde{\omega}^2 - \omega^2}d\tilde{\omega}, \tag{2.10}$$

where CH deontes the *Cauchy principal value*. Inserting 2.9 in 2.8 we get

$$\chi(\omega)'' = cos(\alpha)DR(\omega) + sin(\alpha)\frac{2}{\pi}CH \int_0^\infty \frac{\tilde{\omega}DR(\tilde{\omega})}{\tilde{\omega}^2 - \omega^2}d\tilde{\omega} \tag{2.11}$$

We choose α in a way that the phase corrected $\chi(\omega)''$ can be described by a lorentzian function, which qunatifies the physical parameters of the exciton resonance [10].

Alternatively a quantitative analysis of the excitons resonance could be done using the *transfer matrix method*, which is a powerful and frequently used tool to analyze the propagation of electromagnetic waves through dielectric media with layers of different sucseptibility but goes beyond the scope of the course.

3 Experimental Procedure

1. **Build up the experimental setup and make yourself familiar** with the confocal setup, the sample positioning stage, the spectrometer control and the software.

2. **Finding the focal plane on the sample surface:** Connect the Halogen light source to the excitation fiber, turn on the lamp and bring the sample surface into the focal plane of the microscope by moving the z-screw (vertical screw) of the positioning stage clockwise. To find the focus on the sample surface you can monitor the reflected and collected light with the spy usb camera using a standard usb camera software such as oasis, which is already installed on the computer connected to the setup. **Make sure to not hit the objective with the sample!** The working distance of the objective is 0.3mm, which is not much but still resolvable by bare eye as a small slit between sample and objective surface, when looking at the setup from the side. If the sample gets to close to the objective and the focal spot of the excitation fiber core has not shown up on the spy camera:

   - move the sample back downwards
   - check that the beam path between excitation fiber and objective as well as objective and spy camera is not blocked
   - check whether the camera is running properly (use a flashlight to illuminate the camera from the side an see if the light is detected)
   - approach the objective again moving the sample stage upwards

3. **Orientation on the sample:** Once you found the focus on the sample surface, use the x- and y-screw of the positioning stage to laterally move the sample in the focal plane of the the objective. Fig. 3.1 shows an image of the region of interest on the sample, which is in the center of the silicon wafer. The region of interest is devided into quadrants by gold markers. Try to find orientation by moving along the edges of the gold structure. If the sample is slightly tilted, the surface might move out of the focal plane while moving laterally. In this case, adjust the z-screw of the positioning stage. Here, you can find a video showing the operation of the micrometer stage to bring the sample into the focus of the objective and find orientation on the sample:

4. **Resolution of the microscope:** Move to region **II** (see Fig. 3.1). The hBN layer, which covers the TMD Bilayer has atomically sharp edges. Due to interference effects, the intensity of the light reflected on the hBN surface differs strongly from the intensity of light reflected from the surrounding Si/SiO_2 substrate. Try to optimize the focal position by maximizing the number of counts of the reflected light on the CCD at 790nm. Move stepwise (ideally steps of 1/2 tick on the micrometer screw of the translation stage) from the Si/SiO_2 substrate onto the hBN flake at a sharp edge of the flake. Record a spectrum at every step (spectrometer settings: CW=790nm, integration time = 0.1s, number of spectra = 1, single acquisition).
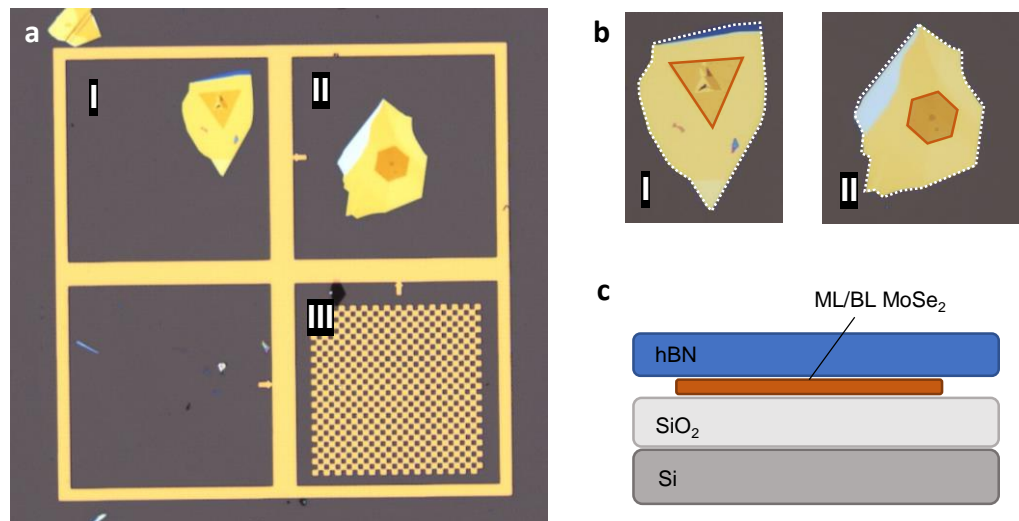
Abbildung 3.1: **Overview of the sample**: **a** Overview of the sample acquired with an optical microscope. Regions of interest are labeled with roman numbers. **b** Region I and II with hBN-covered TMD Mono- and Bilayer, respectively. The TMD layers (highlighted with orange lines) can be easily identified by the change in optical contrast compared to the hBN region (white dotted lines). **c** Schematics of the sample structure.

5. **Scale of the sample:** Move region III on the sample into the focal spot (Fig. 3.1a) where you find a gold chessboard pattern. Move the sample into the focus of the objective. Find out the lattice constant of the pattern by repeating the previous type of measurement, now scanning across a few fields of the gold structure and plot the recorded Intensity trace against the corresponding steps of the micrometer screw. Record an image of the excitation spot on the chessboard pattern. With this you will get an estimate of the size of the excitation spot.

6. **Spectroscopy on the TMD monolayer:**

   - Move back to region I with the TMD monolayer. Try to identify distinctive points of the hBN flake by moving along the edges of the flake and comparing the live image of the spy camera with the microscope image in fig. 3.1. The monolayer is barely visible on the white light reflection image but its position can be estimated when you have orientation on the sample.

   - Switch the configuration of the setup from Reflection to **Photoluminescence**. Flip the optical longpass (Semrock FF01-715/LP-25) and shortpass filter (FESH0700SP) in the excitation and detection arm of the setup into the optical pathway and connect the 685nm laser with the excitation fiber. **Be careful with the open fiber end!** Put one of the green covers onto the open fiber end, then connect the fiber corresponding to the 685nm Laser to the excitation fiber. Make sure that the fiber is connected properly with the connector. **Be careful handling the laser!** Even reflexes off plain metal surfaces (watches, rings, . . .) are

dangerous. You may use protection goggles.

- Turn on the laser and turn the power ajustment knob to the maximum position. Now move slowly across the sample while continuously acquiring with the spectrometer (spectrometer settings: CW=790nm, integration time = 1s, number of spectra = 1, continous acquisition). Once you cross the TMD monolayer a pronounced PL peak should appear in the center of the spectral window. When you found a position with a large number PL counts acquire and save the PL spectrum (spectrometer settings: CW=790nm, integration time = 1s, number of spectra = 10 for better signal to noise ratio (SNR), continous acquisition).

- **Differential Reflection Measurement on the TMD monolayer**: Stay at this position and switch back to reflection configuration (Turn off the 685nm Laser, remove the optical filters and connect the halogen lamp to the excitation fiber). Acquire a reflection spectrum at the same position where you measured PL on the TMD monolayer (spectrometer settings: CW=790nm, integration time = 1s, number of spectra = 10 for better signal to noise ratio (SNR), single acquisition). To calculate the differential relfection and analyse the absoption of the TMD monolayer you need to acquire a background reference spectrum at a position with hBN only. Move the TMD monolayer away from the excitation spot while continously acquiring with the spectrometer, you should see a slight increase of counts once you reach a region with hBN only. Here, repeat the reflection measurement with same measurement condition as on the TMD monolayer. You can do a quick evaluation of the differential reflection spectrum with the corresponding python script. The DR spectrum should look similar to the one plotted in fig.3.2
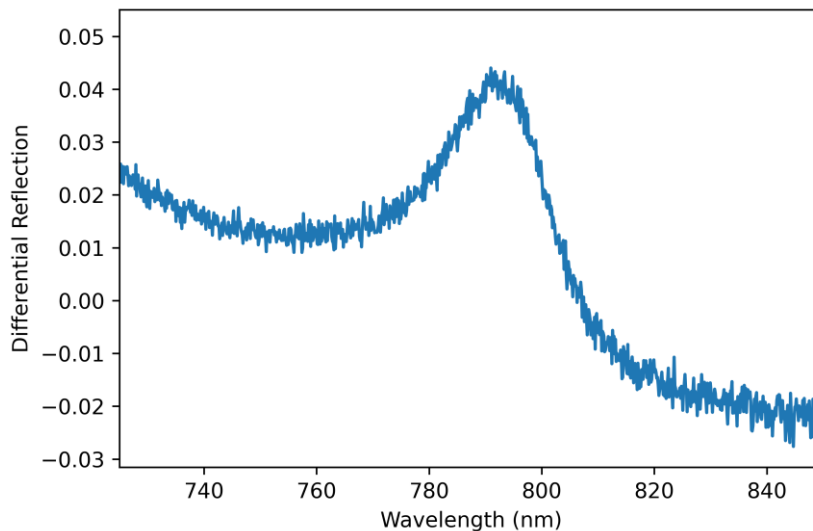

Abbildung 3.2: **DR spectrum on MoSe$_2$ monolayer**

7. **Spectroscopy on the TMD bilayer**: Move region II into the focal spot, where you find a MoSe$_2$ bilayer. Repeat the experimental procedure from the previous point to

measure PL and DR on the bilayer. Do you observe different behaviour compared to the measurement on the monolayer?

Literaturverzeichnis

[1] Geim, A. K.; Grigorieva, I. V. *Nature* **2013,** *499,* 419–425.

[2] Mak, K. F.; Lee, C.; Hone, J.; Shan, J.; Heinz, T. F. *Phys. Rev. Lett.* **2010,** *105,* 136805.

[3] Kormányos, A.; Zólyomi, V.; Drummond, N. D.; Rakyta, P.; Burkard, G.; Fal'ko, V. I. *Phys. Rev. B* **2013,** *88,* 045416.

[4] Deilmann, T.; Thygesen, K. S. *2D Mater.* **2019,** *6,* 035003.

[5] Keldysh, L. V. *JEPT Lett.* **1979,** *29,* 658–661.

[6] Rytova, N. S. *Mosc. Univ. Phys. Bull.* **1967,** *3,* 18.

[7] Chernikov, A.; Berkelbach, T. C.; Hill, H. M.; Rigosi, A.; Li, Y.; Aslan, B.; Reichman, D. R.; Hybertsen, M. S.; Heinz, T. F. *Phys. Rev. Lett.* **2014,** *113,* 076802.

[8] Ren, L.; Robert, C.; Urbaszek, B.; Marie, X.; Semina, M.; Glazov, M. *Comptes Rendus. Physique* **2021,** *22,* 1-10.

[9] Courtade, E. *et al. Phys. Rev. B* **2017,** *96,* 085302.

[10] Back, P.; Sidler, M.; Cotlet, O.; Srivastava, A.; Takemura, N.; Kroner, M.; Imamoğlu, A. *Phys. Rev. Lett.* **2017,** *118,* 237404.